
OpenSTL: A Comprehensive Benchmark of Spatio-Temporal Predictive Learning

Cheng Tan^{1,2*}, Siyuan Li^{1,2*}, Zhangyang Gao^{1,2}, Wenfei Guan³,
Zedong Wang², Zicheng Liu^{1,2}, Lirong Wu^{1,2}, and Stan Z. Li^{2†}

¹Zhejiang University, ³Xidian University

²AI Lab, Research Center for Industries of the Future, Westlake University

Abstract

1 Spatio-temporal predictive learning is a learning paradigm that enables models to
2 learn spatial and temporal patterns by predicting future frames from given past
3 frames in an unsupervised manner. Despite remarkable progress in recent years,
4 a lack of systematic understanding persists due to the diverse settings, complex
5 implementation, and difficult reproducibility. Without standardization, comparisons
6 can be unfair and insights inconclusive. To address this dilemma, we propose
7 OpenSTL, a comprehensive benchmark for spatio-temporal predictive learning that
8 categorizes prevalent approaches into recurrent-based and recurrent-free models.
9 OpenSTL provides a modular and extensible framework implementing various
10 state-of-the-art methods. We conduct standard evaluations on datasets across
11 various domains, including synthetic moving object trajectory, human motion,
12 driving scenes, traffic flow and weather forecasting. Based on our observations,
13 we provide a detailed analysis of how model architecture and dataset properties
14 affect spatio-temporal predictive learning performance. Surprisingly, we find that
15 recurrent-free models achieve a good balance between efficiency and performance
16 than recurrent models. Thus, we further extend the common MetaFormers to boost
17 recurrent-free spatial-temporal predictive learning. We open-source the code and
18 models at github.com/chengtan9907/OpenSTL.

19 1 Introduction

20 Recent years have witnessed rapid and remarkable progress in spatio-temporal predictive learning [35,
21 26, 9, 38]. This burgeoning field aims to learn latent spatial and temporal patterns through the
22 challenging task of forecasting future frames based solely on given past frames in an unsupervised
23 manner [37]. By ingesting raw sequential data, these self-supervised models can uncover intricate
24 spatial and temporal interdependencies without the need for tedious manual annotation, enabling them
25 to extrapolate coherently into the future in a realistic fashion [26, 11]. Spatio-temporal predictive
26 learning benefits a wide range of applications with its ability to anticipate the future from the past in
27 a data-driven way, including modeling the devastating impacts of climate change [35, 32], predicting
28 human movement [55, 42], forecasting traffic flow in transportation systems [7, 48], and learning
29 expressive representations from video [29, 17]. By learning to predict the future without supervision
30 from massive datasets, these techniques have the potential to transform domains where anticipation
31 and planning are crucial but limited labeled data exists [8, 2, 41, 28].

*Equal contribution.

†Corresponding author.

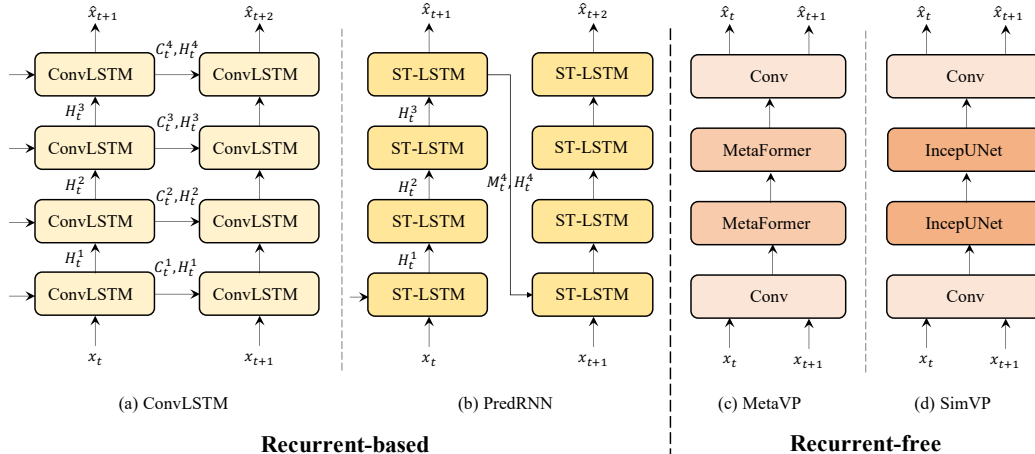


Figure 1: Two typical spatio-temporal predictive learning models.

32 Despite the significance of spatio-temporal predictive learning and the development of various
 33 approaches, there remains a conspicuous lack of a comprehensive benchmark for this field. We
 34 believe that a comprehensive benchmark is essential for advancing the field and facilitating meaningful
 35 comparisons between different methods. In particular, there exists a perennial question that has not
 36 yet been conclusively answered: *is it necessary to employ recurrent neural network architectures*
 37 *to capture temporal dependencies?* In other words, *can recurrent-free models achieve performance*
 38 *comparable to recurrent-based models without explicit temporal modeling?*

39 Since the seminal work ConvLSTM [35] was proposed, which ingeniously integrates convolutional
 40 networks and long-short term memory (LSTM) networks [13] to separately capture spatial and tem-
 41 poral correlations, researchers have vacillated between utilizing or eschewing recurrent architectures.
 42 As shown in Figure 1, (a) ConvLSTM is a prototypical recurrent-based model that infuses a recurrent
 43 structure into convolutional networks. (b) PredRNN [46] represents a series of recurrent models
 44 that revise the flow of information to enhance performance. (c) MetaVP is the recurrent-free model
 45 that abstracted from SimVP by substituting its IncepU [9] modules with MetaFormers [53]. (d)
 46 SimVP [9, 37] is a typical recurrent-free model that achieves performance comparable to previous
 47 state-of-the-art models without explicitly modeling temporal dependencies.

48 In this study, we illuminate the long-standing question of whether explicit temporal modeling
 49 with recurrent neural networks is requisite for spatio-temporal predictive learning. To achieve
 50 this, we present a comprehensive benchmark called OpenSTL (**Open Spatio-Temporal** predictive
 51 **Learning**). We revisit the approaches that represent the foremost strands within a modular and
 52 extensive framework to ensure fair comparisons. We summarize our main contributions as follows:

- 53 • We build OpenSTL, a comprehensive benchmark for spatio-temporal predictive learning
 54 that includes 14 representative algorithms and 24 models. OpenSTL covers a wide range of
 55 methods and classifies them into two categories: recurrent-based and recurrent-free methods.
- 56 • We conduct extensive experiments on a diversity of tasks ranging from synthetic moving
 57 object trajectories to real-world human motion, driving scenes, traffic flow, and weather
 58 forecasting. The datasets span synthetic to real-world data and micro-to-macro scales.
- 59 • While recurrent-based models have been well developed, we rethink the potential
 60 of recurrent-free models based on insights from OpenSTL. We propose generalizing
 61 MetaFormer-like architectures [53] to boost recurrent-free spatio-temporal predictive learn-
 62 ing. Recurrent-free models can thus reformulate the problem as a downstream task of
 63 designing vision backbones for general applications.

64 2 Background and Related work

65 2.1 Problem definition

66 We propose the formal definition for the spatio-temporal predictive learning problem as follows.
67 Given a sequence of video frames $\mathcal{X}^{t,T} = \{\mathbf{x}^i\}_{t-T+1}^t$ up to time t spanning the past T frames, the
68 objective is to predict the subsequent T' frames $\mathcal{Y}^{t+1,T'} = \{\mathbf{x}^i\}_{t+1}^{t+1+T'}$ from time $t + 1$ onwards,
69 where each frame $\mathbf{x}_i \in \mathbb{R}^{C \times H \times W}$ typically comprises C channels, with height H and width W
70 pixels. In practice, we represent the input sequence of observed frames and output sequence of
71 predicted frames respectively as tensors $\mathcal{X}^{t,T} \in \mathbb{R}^{T \times C \times H \times W}$ and $\mathcal{Y}^{t+1,T'} \in \mathbb{R}^{T' \times C \times H \times W}$.

72 The model with learnable parameters Θ learns a mapping $\mathcal{F}_\Theta : \mathcal{X}^{t,T} \mapsto \mathcal{Y}^{t+1,T'}$ by leveraging both
73 spatial and temporal dependencies. In our case, the mapping \mathcal{F}_Θ corresponds to a neural network
74 trained to minimize the discrepancy between the predicted future frames and the ground-truth future
75 frames. The optimal parameters Θ^* are given by:

$$\Theta^* = \arg \min_{\Theta} \mathcal{L}(\mathcal{F}_\Theta(\mathcal{X}^{t,T}), \mathcal{Y}^{t+1,T'}), \quad (1)$$

76 where \mathcal{L} denotes a loss function that quantifies such discrepancy.

77 In this study, we categorize prevalent spatio-temporal predictive learning methods into two classes:
78 recurrent-based and recurrent-free models. For *recurrent-based models*, the mapping \mathcal{F}_Θ comprises
79 several recurrent interactions:

$$\mathcal{F}_\Theta : f_\theta(\mathbf{x}^{t-T+1}, \mathbf{h}^{t-T+1}) \circ \dots \circ f_\theta(\mathbf{x}^t, \mathbf{h}^t) \circ \dots \circ f_\theta(\mathbf{x}^{t+T'-1}, \mathbf{h}^{t+T'-1}), \quad (2)$$

80 where \mathbf{h}^i represents the memory state encompassing historical information and f_θ denotes the
81 mapping between each pair of adjacent frames. The parameters θ are shared across each state.
82 Therefore, the prediction process can be expressed as follows:

$$\mathbf{x}^{t+1} = f_\theta(\mathbf{x}^i, \mathbf{h}^i), \forall i \in \{t+1, \dots, t+T'\}, \quad (3)$$

83 For *recurrent-free* models, the prediction process directly feeds the whole sequence of observed
84 frames into the model and outputs the complete predicted frames at once.

85 2.2 Recurrent-based models

86 Since the pioneering work ConvLSTM [35] was proposed, recurrent-based models [26, 27, 14,
87 11, 52, 28] have been extensively studied. PredRNN [46] adopts vanilla ConvLSTM modules
88 to build a Spatio-temporal LSTM (ST-LSTM) unit that models spatial and temporal variations
89 simultaneously. PredRNN++ [44] proposes a gradient highway unit to mitigate the gradient vanishing
90 and a Casual-LSTM module to cascadelly connect spatial and temporal memories. PredRNNv2 [47]
91 further proposes a curriculum learning strategy and a memory decoupling loss to boost performance.
92 MIM [48] introduces high-order non-stationarity learning in designing LSTM modules. PhyDNet [11]
93 explicitly disentangles PDE dynamics from unknown complementary information with a recurrent
94 physical unit. E3DLSTM [45] integrates 3D convolutions into recurrent networks. MAU [3] proposes
95 a motion-aware unit that captures motion information. Although various recurrent-based models have
96 been developed, the reasons behind their strong performance remain not fully understood.

97 2.3 Recurrent-free models

98 Compared to recurrent-based models, recurrent-free models have received less attention. Previous
99 studies tend to use 3D convolutional networks to model temporal dependencies [25, 1]. PredCNN [51]
100 and TrajectoryCNN [22] use 2D convolutional networks for efficiency. However, early recurrent-
101 free models were doubted due to their poor performance. Recently, SimVP [9, 37, 38] provided
102 a simple but effective recurrent-free baseline with competitive performance. PastNet [50] and
103 IAM4VP [34] are two recent recurrent-free models that perform strong performance. In this study,
104 we implemented representative recurrent-based and recurrent-free models under a unified framework
105 to systematically investigate their intrinsic properties. Moreover, we further explored the potential of
106 recurrent-free models by reformulating the spatio-temporal predictive learning problem and extending
107 MetaFormers [53] to bridge the gap between the visual backbone and spatio-temporal learning.

108 3 OpenSTL

109 3.1 Supported Methods

110 3.1.1 Overview

111 OpenSTL has implemented 14 representative spatio-temporal predictive learning methods under
112 a unified framework, including 11 recurrent-based methods and 3 recurrent-free methods. We
113 summarize these methods in Table 1, where we also provide the corresponding conference/journal
114 and the types of their spatial-temporal modeling components. The spatial modeling of these methods is
115 fundamentally consistent. Most methods apply two-dimensional convolutional networks (Conv2D) to
116 model spatial dependencies, while E3D-LSTM and CrevNet harness three-dimensional convolutional
117 networks (Conv3D) instead.

118 The primary distinction between these methods lies in how they model temporal dependencies
119 using their proposed modules. The ST-LSTM module, proposed in PredRNN [46], is the most
120 widely used module. CrevNet has a similar modeling approach as PredRNN, but it incorporates
121 an information-preserving mechanism into the model. Analogously, Casual-LSTM [44], MIM
122 Block [48], E3D-LSTM [45], PhyCell [11], and MAU [3] represent variants of ConvLSTM proposed
123 with miscellaneous motivations. MVFB is built as a multi-scale voxel flow block that diverges from
124 ConvLSTM. However, DMVFN [15] predicts future frames frame-by-frame which still qualifies as a
125 recurrent-based model. IncepU [9] constitutes an Unet-like module that also exploits the multi-scale
126 feature from the InceptionNet-like architecture. gSTA [37] and TAU [38] extend the IncepU module to
127 simpler and more efficient architectures without InceptionNet or Unet-like architectures. In this work,
128 we further extend the temporal modeling of recurrent-free models by introducing MetaFormers [53]
129 to boost recurrent-free spatio-temporal predictive learning.

Table 1: Categorizations of the supported spatial-temporal predictive learning methods in OpenSTL.

Category	Method	Conference/Journal	Spatial modeling	Temporal modeling
Recurrent-based	ConvLSTM [35]	NeurIPS 2015	Conv2D	Conv-LSTM
	PredNet [26]	ICLR 2017	Conv2D	ST-LSTM
	PredRNN [46]	NeurIPS 2017	Conv2D	ST-LSTM
	PredRNN++ [44]	ICML 2018	Conv2D	Casual-LSTM
	MIM [48]	CVPR 2019	Conv2D	MIM Block
	E3D-LSTM [45]	ICLR 2019	Conv3D	E3D-LSTM
	CrevNet [52]	ICLR 2020	Conv3D	ST-LSTM
	PhyDNet [11]	CVPR 2020	Conv2D	ConvLSTM+PhyCell
	MAU [3]	NeurIPS 2021	Conv2D	MAU
	PredRNNv2 [47]	TPAMI 2022	Conv2D	ST-LSTM
Recurrent-free	DMVFN [15]	CVPR 2023	Conv2D	MVFB
	SimVP [9]	CVPR 2022	Conv2D	IncepU
	TAU [38]	CVPR 2023	Conv2D	TAU
	SimVPv2 [37]	arXiv	Conv2D	gSTA

130 3.1.2 Rethink the recurrent-free models

131 Although less studied, recurrent-free spatio-temporal predictive learning models share a similar
132 architecture, as illustrated in Figure 2. The encoder comprises several 2D convolutional networks,
133 which project high-dimensional input data into a low-dimensional latent space. When given a batch
134 of input observed frames $\mathcal{B} \in \mathbb{R}^{B \times T \times C \times H \times W}$, the encoder focuses solely on intra-frame spatial
135 correlations, ignoring temporal modeling. Subsequently, the middle temporal module stacks the
136 low-dimensional representations along the temporal dimension to ascertain temporal dependencies.
137 Finally, the decoder comprises several 2D convolutional upsampling networks, which reconstruct
138 subsequent frames from the learned latent representations.

139 The encoder and decoder enable efficient temporal learning by modeling temporal dependencies
 140 in a low-dimensional latent space. The core component of recurrent-free models is the temporal
 141 module. Previous studies have proposed temporal modules such as IncepU [9], TAU [38], and
 142 gSTA [37] that have proved beneficial. However, we argue that the competence stems primarily
 143 from the general recurrent-free architecture instead of the specific temporal modules. Thus, we
 144 employ MetaFormers [53] as the temporal module by changing the input channels from the original
 145 C to inter-frame channels $T \times C$. By extending the recurrent-free architecture, we leverage the
 146 advantages of MetaFormers to enhance the recurrent-free model. In this work, we implement
 147 ViT [6], Swin Transformer [23], Uniformer [19], MLP-Mixer [39], ConvMixer [40], Poolformer [53],
 148 ConvNeXt [24], VAN [12], HorNet [30], and MogaNet [20] for the MetaFormers-based recurrent-free
 149 model, substituting the intermediate temporal module in the original recurrent-free architecture.

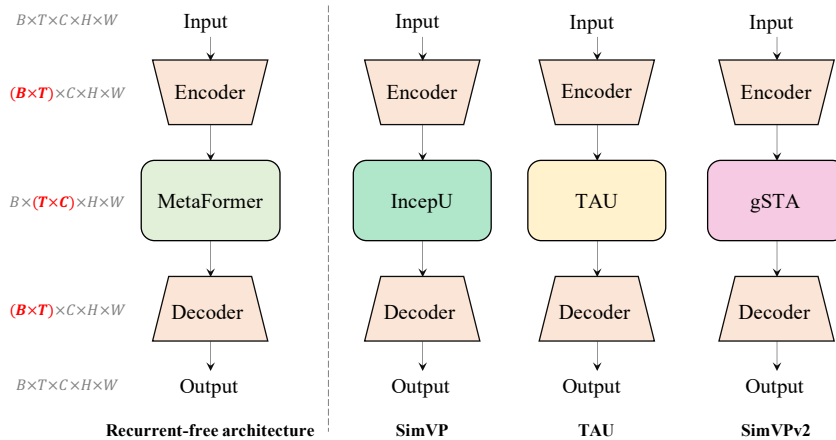


Figure 2: The general architecture of recurrent-free models.

150 3.2 Supported Tasks

151 We have curated five diverse tasks in our OpenSTL benchmark, which cover a wide range of scenarios
 152 from synthetic simulations to real-world situations at various scales. The tasks include: synthetic
 153 moving object trajectories, real-world human motion capture, driving scenes, traffic flow, and weather
 154 forecasting. The datasets used in our benchmark range from synthetic to real-world, and from micro
 155 to macro scales. We have provided a summary of the dataset statistics in Table 2.

Table 2: The detailed dataset statistics of the supported tasks in OpenSTL.

Dataset	Training size	Testing size	Channel	Height	Width	T	T'
Moving MNIST	10,000	10,000	1	64	64	10	10
KTH	4,940	3,030	1	128	128	10	20/40
Human3.6M	73,404	8,582	3	128	128	4	4
Kitti&Caltech	3,160	3,095	3	128	160	10	1
TaxiBJ	20,461	500	2	32	32	4	4
WeatherBench-S	2,167	706	1	32/128	64/256	12	12
WeatherBench-M	54,019	2,883	4	32	64	4	4

156 **Synthetic moving object trajectory prediction** *Moving MNIST* [36] is one of the seminal benchmark
 157 datasets that has been extensively utilized. Each video sequence comprises two moving digits confined
 158 within a 64×64 frame. Each digit was assigned a velocity whose direction was randomly chosen
 159 from a unit circle and whose magnitude was also arbitrarily selected from a fixed range. Apart from
 160 the original Moving MNIST dataset, we provide two variants with more complicated objects (*Moving*
 161 *FashionMNIST*) that replace the digits with fashion objects and more complex scenes (*Moving*
 162 *MNIST-CIFAR*) that employ images from the CIFAR-10 dataset [18] as the background.

163 **Human motion capture** Predicting human motion is challenging due to the complexity of human
164 movements, which vary greatly among individuals and actions. We utilized the *KTH* dataset [33],
165 which includes six types of human actions: walking, jogging, running, boxing, hand waving, and hand
166 clapping. We furnish two settings, predicting the next 20 and 40 frames respectively. *Human3.6M* [16]
167 is an intricate human pose dataset containing high-resolution RGB videos. Analogous to preceding
168 studies [11, 48], we predict the next four frames by the observed four frames.

169 **Driving scene prediction** Predicting the future dynamics of driving scenarios is crucial for au-
170 tonomous driving. Compared to other tasks, this undertaking involves non-stationary and diverse
171 scenes. To address this issue, we follow the conventional approach [26] and train the model on the
172 *Kitti* [10] dataset. We then evaluate the performance on the *Caltech Pedestrian* [5] dataset. To ensure
173 consistency, we center-cropped and downsized all frames to 128×160 pixels.

174 **Traffic flow prediction** Forecasting the dynamics of crowds is crucial for traffic management and
175 public safety. To evaluate spatio-temporal predictive learning approaches for traffic flow prediction,
176 we use the *TaxiBJ* [54] dataset. This dataset includes GPS data from taxis and meteorological data
177 in Beijing. The dataset contains two types of crowd flows, representing inflow and outflow. The
178 temporal interval is 30 minutes, and the spatial resolution is 32×32 .

179 **Weather forecasting** Global weather pattern prediction is an essential natural predicament. The
180 WeatherBench [31] dataset is a large-scale weather forecasting dataset encompassing various types
181 of climatic factors. The raw data is re-grid to 5.625° resolution (32×64 grid points) and 1.40625°
182 (128×256 grid points). We consider two setups: First, *WeatherBench-S* is a single-variable setup in
183 which each climatic factor is trained independently. The model is trained on data from 2010-2015,
184 validated on data from 2016, and tested on data from 2017-2018, with a one-hour temporal interval.
185 Second, *WeatherBench-M* is a multi-variable setup that mimics real-world weather forecasting more
186 closely. All climatic factors are trained simultaneously. The model is trained on data from 1979
187 to 2015, using the same validation and testing data as WeatherBench-S. The temporal interval is
188 extended to six hours, capturing a broader range of temporal dependencies.

189 3.3 Evaluation Metrics

190 We evaluate the performance of supported models on the aforementioned tasks using various metrics
191 in a thorough and rigorous manner. We use them for specific tasks according to their characteristics.

192 **Error metrics** We utilize the mean squared error (MSE) and mean absolute error (MAE) to evaluate
193 the difference between the predicted results and the true targets. Root mean squared error (RMSE) is
194 also used in weather forecasting as it is more common in this domain.

195 **Similarity metrics** We utilize the structural similarity index measure (SSIM) [49] and peak signal-to-
196 noise ratio (PSNR) to evaluate the similarity between the predicted results and the true targets. Such
197 metrics are extensively used in image processing and computer vision.

198 **Perceptual metrics** LPIPS [56] is implemented to evaluate the perceptual difference between the
199 predicted results and the true targets in the human visual system. LPIPS provides a perceptually-
200 aligned evaluation for vision tasks. We utilize this metric in real-world video prediction tasks.

201 **Computational metrics** We utilize the number of parameters and the number of floating-point
202 operations (FLOPs) to evaluate the computational complexity of the models. We also report the
203 frames per second (FPS) on a single NVIDIA V100 GPU to evaluate the inference speed.

204 3.4 Codebase Structure

205 While existing open-sourced spatio-temporal predictive learning codebases are independent, OpenSTL
206 provides a modular and extensible framework that adheres to the design principles of OpenMMLab [4]
207 and assimilates code elements from OpenMixup [21] and USB [43]. OpenSTL excels in user-
208 friendliness, organization, and comprehensiveness, surpassing the usability of existing open-source
209 STL codebases. A detailed description of the codebase structure can be found in Appendix B.

210 **4 Experiment and Analysis**

211 We conducted comprehensive experiments on the mentioned tasks to assess the performance of the
 212 supported methods in OpenSTL. Detailed analysis of the results is presented to gain insights into
 213 spatio-temporal predictive learning. Implementation details can be found in Appendix C.

214 **4.1 Synthetic Moving Object Trajectory Prediction**

215 We conduct experiments on the synthetic moving object trajectory prediction task, utilizing three
 216 datasets: Moving MNIST, Moving FashionMNIST, and Moving MNIST-CIFAR. The performance of
 217 the evaluated models on the Moving MNIST dataset is reported in Table 3. The detailed results for
 218 the other two synthetic datasets are in Appendix D.1.

219 It can be observed that recurrent-based models yield varied results that do not consistently outperform
 220 recurrent-free models, while recurrent-based models always exhibit slower inference speeds than their
 221 recurrent-free counterparts. Although PredRNN, PredRNN++, MIM, and PredRNNv2 achieve lower
 222 MSE and MAE values compared to recurrent-free models, their FLOPs are nearly five times higher,
 223 and their FPS are approximately seven times slower than all recurrent-free models. Furthermore, there
 224 are minimal disparities in the performance of recurrent-free models as opposed to recurrent-based
 225 models, highlighting the robustness of the proposed general recurrent-free architecture. The remaining
 226 two synthetic datasets, consisting of more intricate moving objects (Moving FashionMNIST) and
 227 complex scenes (Moving MNIST-CIFAR), reinforce the experimental findings that recurrent-free
 228 models deliver comparable performance with significantly higher efficiency. In these toy datasets
 229 characterized by high frequency but low resolution, recurrent-based models excel in capturing
 230 temporal dependencies but are susceptible to high computational complexity.

Table 3: The performance on the Moving MNIST dataset.

	Method	Params (M)	FLOPs (G)	FPS	MSE ↓	MAE ↓	SSIM ↑	PSNR ↑
Recurrent-based	ConvLSTM	15.0	56.8	113	29.80	90.64	0.9288	22.10
	PredNet	12.5	8.4	659	161.38	201.16	0.7783	14.67
	PredRNN	23.8	116.0	54	23.97	72.82	0.9462	23.28
	PredRNN++	38.6	171.7	38	22.06	69.58	0.9509	23.65
	MIM	38.0	179.2	37	22.55	69.97	0.9498	23.56
	E3D-LSTM	51.0	298.9	18	35.97	78.28	0.9320	21.11
	CrevNet	5.0	270.7	10	30.15	86.28	0.9350	22.15
	PhyDNet	3.1	15.3	182	28.19	78.64	0.9374	22.62
	MAU	4.5	17.8	201	26.86	78.22	0.9398	22.57
	PredRNNv2	23.9	116.6	52	24.13	73.73	0.9453	23.21
Recurrent-free	DMVFN	3.5	0.2	1145	123.67	179.96	0.8140	16.15
	SimVP	58.0	19.4	209	32.15	89.05	0.9268	21.84
	TAU	44.7	16.0	283	24.60	71.93	0.9454	23.19
	SimVPv2	46.8	16.5	282	26.69	77.19	0.9402	22.78
	ViT	46.1	16.9	290	35.15	95.87	0.9139	21.67
	Swin Transformer	46.1	16.4	294	29.70	84.05	0.9331	22.22
	Uniformer	44.8	16.5	296	30.38	85.87	0.9308	22.13
	MLP-Mixer	38.2	14.7	334	29.52	83.36	0.9338	22.22
	ConvMixer	3.9	5.5	658	32.09	88.93	0.9259	21.93
	Poolformer	37.1	14.1	341	31.79	88.48	0.9271	22.03
	ConvNext	37.3	14.1	344	26.94	77.23	0.9397	22.74
	VAN	44.5	16.0	288	26.10	76.11	0.9417	22.89
	HorNet	45.7	16.3	287	29.64	83.26	0.9331	22.26
MogaNet	46.8	16.5	255	25.57	75.19	0.9429	22.99	

231 **4.2 Real-world Video Prediction**

232 We perform experiments on real-world video predictions, specifically focusing on human motion
 233 capturing using the KTH and Human3.6M datasets, as well as driving scene prediction using the
 234 Kitti&Caltech dataset. Due to space constraints, we present the results for the Kitti&Caltech dataset
 235 in Table 4, while the detailed results for the other datasets can be found in Appendix D.2. We observed
 236 that as the resolution increases, the computational complexity of recurrent-based models dramatically
 237 increases. In contrast, recurrent-free models achieve a commendable balance between efficiency and
 238 performance. Notably, although some recurrent-based models achieve lower MSE and MAE values,
 239 their FLOPs are nearly 20 times higher compared to their recurrent-free counterparts. This highlights
 240 the efficiency advantage of recurrent-free models, especially in high-resolution scenarios.

Table 4: The performance on the Kitti&Caltech dataset.

Method	Params (M)	FLOPs (G)	FPS	MSE ↓	MAE ↓	SSIM ↑	PSNR ↑	LPIPS ↓	
Recurrent-based	ConvLSTM	15.0	595.0	33	139.6	1583.3	0.9345	27.46	8.58
	PredNet	12.5	42.8	94	159.8	1568.9	0.9286	27.21	11.29
	PredRNN	23.7	1216.0	17	130.4	1525.5	0.9374	27.81	7.40
	PredRNN++	38.5	1803.0	12	125.5	1453.2	0.9433	28.02	13.21
	MIM	49.2	1858.0	39	125.1	1464.0	0.9409	28.10	6.35
	E3D-LSTM	54.9	1004.0	10	200.6	1946.2	0.9047	25.45	12.60
	PhyDNet	3.10	40.4	117	312.2	2754.8	0.8615	23.26	32.19
	MAU	24.3	172.0	16	177.8	1800.4	0.9176	26.14	9.67
	PredRNNv2	23.8	1223.0	16	147.8	1610.5	0.9330	27.12	8.92
	DMVFN	3.6	1.2	557	183.9	1531.1	0.9314	26.78	4.94
Recurrent-free	SimVP	8.6	60.6	57	160.2	1690.8	0.9338	26.81	6.76
	TAU	15.0	92.5	55	131.1	1507.8	0.9456	27.83	5.49
	SimVPv2	15.6	96.3	40	129.7	1507.7	0.9454	27.89	5.57
	ViT	12.7	155.0	25	146.4	1615.8	0.9379	27.43	6.66
	Swin Transformer	15.3	95.2	49	155.2	1588.9	0.9299	27.25	8.11
	Uniformer	11.8	104.0	28	135.9	1534.2	0.9393	27.66	6.87
	MLP-Mixer	22.2	83.5	60	207.9	1835.9	0.9133	26.29	7.75
	ConvMixer	1.5	23.1	129	174.7	1854.3	0.9232	26.23	7.76
	Poolformer	12.4	79.8	51	153.4	1613.5	0.9334	27.38	7.00
	ConvNext	12.5	80.2	54	146.8	1630.0	0.9336	27.19	6.99
	VAN	14.9	92.5	41	127.5	1476.5	0.9462	27.98	5.50
	HorNet	15.3	94.4	43	152.8	1637.9	0.9365	27.09	6.00
	MogaNet	15.6	96.2	36	131.4	1512.1	0.9442	27.79	5.39

241 **4.3 Traffic and Weather Forecasting**

242 Traffic flow prediction and weather forecasting are two critical tasks that have significant implications
 243 for public safety and scientific research. While these tasks operate at a macro level, they exhibit
 244 lower frequencies compared to the tasks mentioned above, and the states along the timeline tend to be
 245 more stable. Capturing subtle changes in such tasks poses a significant challenge. In order to assess
 246 the performance of the supported models in OpenSTL, we conduct experiments on the TaxiBJ and
 247 WeatherBench datasets. It is worth noting that weather forecasting encompasses various settings, and
 248 we provide detailed results of them in Appendix D.3.

249 Here, we present a comparison of the MAE and RMSE metrics for representative approaches in
 250 single-variable weather factor forecasting at low resolution. Figure 3 displays the results for four
 251 climatic factors, i.e., temperature, humidity, wind component, and cloud cover. Notably, recurrent-
 252 free models consistently outperform recurrent-based models across all weather factors, indicating
 253 their potential to apply spatio-temporal predictive learning to macro-scale tasks instead of relying
 254 solely on recurrent-based models. These findings underscore the promising nature of recurrent-free
 255 models and suggest that they can be a viable alternative to the prevailing recurrent-based models in
 256 the context of weather forecasting. Furthermore, in the Appendix, we provide additional insights into
 257 high-resolution and multi-variable weather forecasting, where similar trends are observed.

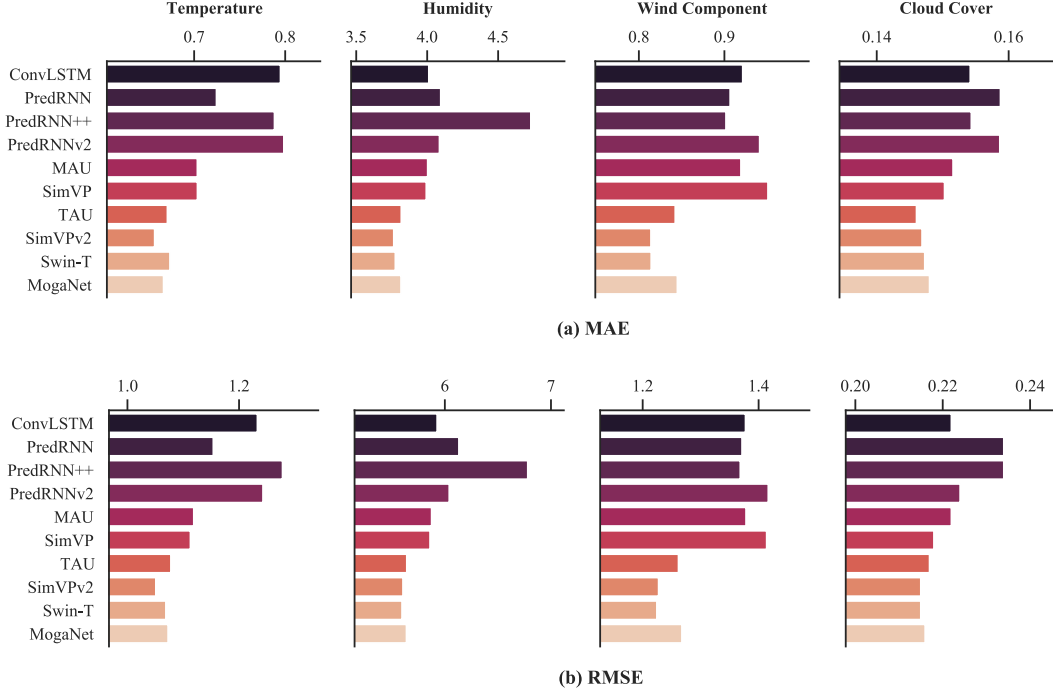


Figure 3: The (a) MAE and (b) RMSE metrics of the representative approaches on the four weather forecasting tasks in WeatherBench.

258 5 Conclusion and Discussion

259 This paper introduces OpenSTL, a comprehensive benchmark for spatio-temporal predictive learning
 260 with a diverse set of 14 representative methods and 24 models, addressing a wide range of challenging
 261 tasks. OpenSTL categorizes existing approaches into recurrent-based and recurrent-free models.
 262 To unlock the potential of recurrent-free models, we propose a general recurrent-free architecture
 263 and introduce MetaFormers for temporal modeling. Extensive experiments are conducted to sys-
 264 tematically evaluate the performance of the supported models across various tasks. In synthetic
 265 datasets, recurrent-based models excel at capturing temporal dependencies, while recurrent-free
 266 models achieve comparable performance with significantly higher efficiency. In real-world video
 267 prediction tasks, recurrent-free models strike a commendable balance between efficiency and perfor-
 268 mance. Additionally, recurrent-free models demonstrate significant superiority over their counterparts
 269 in weather forecasting, highlighting their potential for scientific applications at a macro-scale level.

270 Moreover, we observed that *recurrent architectures are beneficial in capturing temporal dependencies,*
 271 *but they are not always necessary, especially for computationally expensive tasks.* Recurrent-free mod-
 272 els can be a viable alternative that provides a good balance between efficiency and performance. The
 273 effectiveness of recurrent-based models in capturing high-frequency spatio-temporal dependencies
 274 can be attributed to their sequential tracking of frame-by-frame changes, providing a local temporal
 275 inductive bias. On the other hand, recurrent-free models combine multiple frames together, exhibiting
 276 a global temporal inductive bias that is suitable for low-frequency spatio-temporal dependencies. We
 277 hope that our work provides valuable insights and serves as a reference for future research.

278 While our primary focus lies in general spatio-temporal predictive learning, there are still several open
 279 problems that require further investigation. One particular challenge is finding ways to effectively
 280 leverage the strengths of both recurrent-based and recurrent-free models to enhance the modeling of
 281 spatial-temporal dependencies. While there is a correspondence between the spatial encoding and
 282 temporal modeling in MetaVP and the token mixing and channel mixing in MetaFormer, it raises the
 283 question of whether we can improve recurrent-free models by extending the existing MetaFormers.

284 Acknowledgments and Disclosure of Funding

285 This work was supported by the National Key R&D Program of China (2022ZD0115100), the National
286 Natural Science Foundation of China (U21A20427), the Competitive Research Fund (WU2022A009)
287 from the Westlake Center for Synthetic Biology and Integrated Bioengineering.

288 References

- 289 [1] S. Aigner and M. Körner. Futuregan: Anticipating the future frames of video sequences
290 using spatio-temporal 3d convolutions in progressively growing gans. *arXiv preprint*
291 *arXiv:1810.01325*, 2018.
- 292 [2] L. Castrejon, N. Ballas, and A. Courville. Improved conditional vrns for video prediction. In
293 *Proceedings of the IEEE/CVF International Conference on Computer Vision*, pages 7608–7617,
294 2019.
- 295 [3] Z. Chang, X. Zhang, S. Wang, S. Ma, Y. Ye, X. Xinguang, and W. Gao. Mau: A motion-aware
296 unit for video prediction and beyond. *Advances in Neural Information Processing Systems*, 34,
297 2021.
- 298 [4] M. Contributors. MMCV: OpenMMLab computer vision foundation. [https://github.com/
299 open-mmlab/mmcv](https://github.com/open-mmlab/mmcv), 2018.
- 300 [5] P. Dollár, C. Wojek, B. Schiele, and P. Perona. Pedestrian detection: A benchmark. In *CVPR*,
301 June 2009.
- 302 [6] A. Dosovitskiy, L. Beyer, A. Kolesnikov, D. Weissenborn, X. Zhai, T. Unterthiner, M. Dehghani,
303 M. Minderer, G. Heigold, S. Gelly, et al. An image is worth 16x16 words: Transformers for
304 image recognition at scale. In *International Conference on Learning Representations*.
- 305 [7] S. Fang, Q. Zhang, G. Meng, S. Xiang, and C. Pan. Gstnet: Global spatial-temporal network for
306 traffic flow prediction. In *IJCAI*, pages 2286–2293, 2019.
- 307 [8] C. Finn, I. Goodfellow, and S. Levine. Unsupervised learning for physical interaction through
308 video prediction. *Advances in Neural Information Processing Systems*, 29, 2016.
- 309 [9] Z. Gao, C. Tan, and S. Z. Li. Simvp: Simpler yet better video prediction. In *Proceedings of the*
310 *IEEE/CVF Conference on Computer Vision and Pattern Recognition*, pages 3170–3180, 2022.
- 311 [10] A. Geiger, P. Lenz, C. Stiller, and R. Urtasun. Vision meets robotics: The kitti dataset. *The*
312 *International Journal of Robotics Research*, 32(11):1231–1237, 2013.
- 313 [11] V. L. Guen and N. Thome. Disentangling physical dynamics from unknown factors for unsuper-
314 vised video prediction. In *Proceedings of the IEEE/CVF Conference on Computer Vision and*
315 *Pattern Recognition*, pages 11474–11484, 2020.
- 316 [12] M.-H. Guo, C.-Z. Lu, Z.-N. Liu, M.-M. Cheng, and S.-M. Hu. Visual attention network. *arXiv*
317 *preprint arXiv:2202.09741*, 2022.
- 318 [13] S. Hochreiter and J. Schmidhuber. Long short-term memory. *Neural computation*, 9(8):1735–
319 1780, 1997.
- 320 [14] J.-T. Hsieh, B. Liu, D.-A. Huang, L. F. Fei-Fei, and J. C. Niebles. Learning to decompose and
321 disentangle representations for video prediction. *Advances in Neural Information Processing*
322 *Systems*, 31, 2018.
- 323 [15] X. Hu, Z. Huang, A. Huang, J. Xu, and S. Zhou. A dynamic multi-scale voxel flow network for
324 video prediction. In *Proceedings of the IEEE/CVF Conference on Computer Vision and Pattern*
325 *Recognition (CVPR)*, 2023.
- 326 [16] C. Ionescu, D. Papava, V. Olaru, and C. Sminchisescu. Human3.6m: Large scale datasets and
327 predictive methods for 3d human sensing in natural environments. *IEEE transactions on pattern*
328 *analysis and machine intelligence*, 36(7):1325–1339, 2013.

- 329 [17] S. Jenni, G. Meishvili, and P. Favaro. Video representation learning by recognizing temporal
330 transformations. In *European Conference on Computer Vision*, pages 425–442. Springer, 2020.
- 331 [18] A. Krizhevsky, G. Hinton, et al. Learning multiple layers of features from tiny images. 2009.
- 332 [19] K. Li, Y. Wang, J. Zhang, P. Gao, G. Song, Y. Liu, H. Li, and Y. Qiao. Uniformer: Unifying
333 convolution and self-attention for visual recognition. *arXiv preprint arXiv:2201.09450*, 2022.
- 334 [20] S. Li, Z. Wang, Z. Liu, C. Tan, H. Lin, D. Wu, Z. Chen, J. Zheng, and S. Z. Li. Efficient
335 multi-order gated aggregation network. *arXiv preprint arXiv:2211.03295*, 2022.
- 336 [21] S. Li, Z. Wang, Z. Liu, D. Wu, C. Tan, and S. Z. Li. Openmixup: Open mixup toolbox and
337 benchmark for visual representation learning. *ArXiv*, abs/2209.04851, 2022.
- 338 [22] X. Liu, J. Yin, J. Liu, P. Ding, J. Liu, and H. Liu. Trajectorycnn: a new spatio-temporal feature
339 learning network for human motion prediction. *IEEE Transactions on Circuits and Systems for
340 Video Technology*, 31(6):2133–2146, 2020.
- 341 [23] Z. Liu, Y. Lin, Y. Cao, H. Hu, Y. Wei, Z. Zhang, S. Lin, and B. Guo. Swin transformer:
342 Hierarchical vision transformer using shifted windows. In *Proceedings of the IEEE/CVF
343 International Conference on Computer Vision*, pages 10012–10022, 2021.
- 344 [24] Z. Liu, H. Mao, C.-Y. Wu, C. Feichtenhofer, T. Darrell, and S. Xie. A convnet for the 2020s.
345 *arXiv preprint arXiv:2201.03545*, 2022.
- 346 [25] Z. Liu, R. A. Yeh, X. Tang, Y. Liu, and A. Agarwala. Video frame synthesis using deep
347 voxel flow. In *Proceedings of the IEEE International Conference on Computer Vision*, pages
348 4463–4471, 2017.
- 349 [26] W. Lotter, G. Kreiman, and D. Cox. Deep predictive coding networks for video prediction and
350 unsupervised learning. In *International Conference on Learning Representations*, 2017.
- 351 [27] M. Oliu, J. Selva, and S. Escalera. Folded recurrent neural networks for future video prediction.
352 In *Proceedings of the European Conference on Computer Vision (ECCV)*, pages 716–731, 2018.
- 353 [28] S. Oprea, P. Martinez-Gonzalez, A. Garcia-Garcia, J. A. Castro-Vargas, S. Orts-Escolano,
354 J. Garcia-Rodriguez, and A. Argyros. A review on deep learning techniques for video prediction.
355 *IEEE Transactions on Pattern Analysis and Machine Intelligence*, 2020.
- 356 [29] R. Qian, T. Meng, B. Gong, M.-H. Yang, H. Wang, S. Belongie, and Y. Cui. Spatiotemporal
357 contrastive video representation learning. In *Proceedings of the IEEE/CVF Conference on
358 Computer Vision and Pattern Recognition*, pages 6964–6974, 2021.
- 359 [30] Y. Rao, W. Zhao, Y. Tang, J. Zhou, S. N. Lim, and J. Lu. Hornet: Efficient high-order spatial
360 interactions with recursive gated convolutions. *Advances in Neural Information Processing
361 Systems*, 35:10353–10366, 2022.
- 362 [31] S. Rasp, P. D. Dueben, S. Scher, J. A. Weyn, S. Mouatadid, and N. Thuerey. Weatherbench:
363 a benchmark data set for data-driven weather forecasting. *Journal of Advances in Modeling
364 Earth Systems*, 12(11):e2020MS002203, 2020.
- 365 [32] M. Reichstein, G. Camps-Valls, B. Stevens, M. Jung, J. Denzler, N. Carvalhais, et al. Deep
366 learning and process understanding for data-driven earth system science. *Nature*, 566(7743):195–
367 204, 2019.
- 368 [33] C. Schuldt, I. Laptev, and B. Caputo. Recognizing human actions: a local svm approach. In
369 *Proceedings of the 17th International Conference on Pattern Recognition, 2004. ICPR 2004.*,
370 volume 3, pages 32–36. IEEE, 2004.
- 371 [34] M. Seo, H. Lee, D. Kim, and J. Seo. Implicit stacked autoregressive model for video prediction.
372 *arXiv preprint arXiv:2303.07849*, 2023.
- 373 [35] X. Shi, Z. Chen, H. Wang, D.-Y. Yeung, W.-K. Wong, and W.-c. Woo. Convolutional lstm
374 network: A machine learning approach for precipitation nowcasting. *Advances in Neural
375 Information Processing Systems*, 28, 2015.

- 376 [36] N. Srivastava, E. Mansimov, and R. Salakhudinov. Unsupervised learning of video representa-
377 tions using lstms. In *International conference on machine learning*, pages 843–852. PMLR,
378 2015.
- 379 [37] C. Tan, Z. Gao, S. Li, and S. Z. Li. Simvp: Towards simple yet powerful spatiotemporal
380 predictive learning. *arXiv preprint arXiv:2211.12509*, 2022.
- 381 [38] C. Tan, Z. Gao, L. Wu, Y. Xu, J. Xia, S. Li, and S. Z. Li. Temporal attention unit: Towards
382 efficient spatiotemporal predictive learning. In *Proceedings of the IEEE/CVF Conference on*
383 *Computer Vision and Pattern Recognition*, 2023.
- 384 [39] I. O. Tolstikhin, N. Houlsby, A. Kolesnikov, L. Beyer, X. Zhai, T. Unterthiner, J. Yung, A. Steiner,
385 D. Keysers, J. Uszkoreit, et al. Mlp-mixer: An all-mlp architecture for vision. *Advances in*
386 *neural information processing systems*, 34:24261–24272, 2021.
- 387 [40] A. Trockman and J. Z. Kolter. Patches are all you need? *arXiv:2201.09792*, 2022.
- 388 [41] R. Villegas, D. Erhan, H. Lee, et al. Hierarchical long-term video prediction without supervision.
389 In *International Conference on Machine Learning*, pages 6038–6046. PMLR, 2018.
- 390 [42] P. Wang, W. Li, P. Ogunbona, J. Wan, and S. Escalera. Rgb-d-based human motion recognition
391 with deep learning: A survey. *Computer Vision and Image Understanding*, 171:118–139, 2018.
- 392 [43] Y. Wang, H. Chen, Y. Fan, W. Sun, R. Tao, W. Hou, R. Wang, L. Yang, Z. Zhou, L.-Z. Guo,
393 et al. Usb: A unified semi-supervised learning benchmark for classification. *Advances in Neural*
394 *Information Processing Systems*, 35:3938–3961, 2022.
- 395 [44] Y. Wang, Z. Gao, M. Long, J. Wang, and S. Y. Philip. Predrnn++: Towards a resolution of the
396 deep-in-time dilemma in spatiotemporal predictive learning. In *International Conference on*
397 *Machine Learning*, pages 5123–5132. PMLR, 2018.
- 398 [45] Y. Wang, L. Jiang, M.-H. Yang, L.-J. Li, M. Long, and L. Fei-Fei. Eidetic 3d lstm: A model for
399 video prediction and beyond. In *International conference on learning representations*, 2018.
- 400 [46] Y. Wang, M. Long, J. Wang, Z. Gao, and P. S. Yu. Predrnn: Recurrent neural networks for
401 predictive learning using spatiotemporal lstms. *Advances in Neural Information Processing*
402 *Systems*, 30, 2017.
- 403 [47] Y. Wang, H. Wu, J. Zhang, Z. Gao, J. Wang, P. S. Yu, and M. Long. Predrnn: A recurrent neural
404 network for spatiotemporal predictive learning. *arXiv preprint arXiv:2103.09504*, 2021.
- 405 [48] Y. Wang, J. Zhang, H. Zhu, M. Long, J. Wang, and P. S. Yu. Memory in memory: A predictive
406 neural network for learning higher-order non-stationarity from spatiotemporal dynamics. In
407 *Proceedings of the IEEE/CVF Conference on Computer Vision and Pattern Recognition*, pages
408 9154–9162, 2019.
- 409 [49] Z. Wang, A. C. Bovik, H. R. Sheikh, and E. P. Simoncelli. Image quality assessment: from error
410 visibility to structural similarity. *IEEE transactions on image processing*, 13(4):600–612, 2004.
- 411 [50] H. Wu, W. Xion, F. Xu, X. Luo, C. Chen, X.-S. Hua, and H. Wang. Pastnet: Introducing physical
412 inductive biases for spatio-temporal video prediction. *arXiv preprint arXiv:2305.11421*, 2023.
- 413 [51] Z. Xu, Y. Wang, M. Long, J. Wang, and M. KLiss. Predcnn: Predictive learning with cascade
414 convolutions. In *IJCAI*, pages 2940–2947, 2018.
- 415 [52] W. Yu, Y. Lu, S. Easterbrook, and S. Fidler. Efficient and information-preserving future frame
416 prediction and beyond. In *International Conference on Learning Representations*, 2019.
- 417 [53] W. Yu, M. Luo, P. Zhou, C. Si, Y. Zhou, X. Wang, J. Feng, and S. Yan. Metaformer is actually
418 what you need for vision. In *Proceedings of the IEEE/CVF conference on computer vision and*
419 *pattern recognition*, pages 10819–10829, 2022.
- 420 [54] J. Zhang, Y. Zheng, and D. Qi. Deep spatio-temporal residual networks for citywide crowd
421 flows prediction. In *Thirty-first AAAI conference on artificial intelligence*, 2017.
- 422 [55] L. Zhang, G. Zhu, P. Shen, J. Song, S. Afaq Shah, and M. Bennamoun. Learning spatiotemporal
423 features using 3dcnn and convolutional lstm for gesture recognition. In *Proceedings of the IEEE*
424 *International Conference on Computer Vision Workshops*, pages 3120–3128, 2017.

425 [56] R. Zhang, P. Isola, A. A. Efros, E. Shechtman, and O. Wang. The unreasonable effectiveness of
426 deep features as a perceptual metric. In *Proceedings of the IEEE conference on computer vision
427 and pattern recognition*, pages 586–595, 2018.

428 Checklist

429 The checklist follows the references. Please read the checklist guidelines carefully for information on
430 how to answer these questions. For each question, change the default **[TODO]** to **[Yes]**, **[No]**, or
431 **[N/A]**. You are strongly encouraged to include a **justification to your answer**, either by referencing
432 the appropriate section of your paper or providing a brief inline description.

433 Please do not modify the questions and only use the provided macros for your answers. Note that the
434 Checklist section does not count towards the page limit. In your paper, please delete this instructions
435 block and only keep the Checklist section heading above along with the questions/answers below.

- 436 1. For all authors...
 - 437 (a) Do the main claims made in the abstract and introduction accurately reflect the paper’s
438 contributions and scope? **[Yes]**
 - 439 (b) Did you describe the limitations of your work? **[Yes]**
 - 440 (c) Did you discuss any potential negative societal impacts of your work? **[Yes]**
 - 441 (d) Have you read the ethics review guidelines and ensured that your paper conforms to
442 them? **[Yes]**
- 443 2. If you are including theoretical results...
 - 444 (a) Did you state the full set of assumptions of all theoretical results? **[N/A]**
 - 445 (b) Did you include complete proofs of all theoretical results? **[N/A]**
- 446 3. If you ran experiments (e.g. for benchmarks)...
 - 447 (a) Did you include the code, data, and instructions needed to reproduce the main experi-
448 mental results (either in the supplemental material or as a URL)? **[Yes]**
 - 449 (b) Did you specify all the training details (e.g., data splits, hyperparameters, how they
450 were chosen)? **[Yes]** See Appendix C.
 - 451 (c) Did you report error bars (e.g., with respect to the random seed after running experi-
452 ments multiple times)? **[No]**
 - 453 (d) Did you include the total amount of compute and the type of resources used (e.g., type
454 of GPUs, internal cluster, or cloud provider)? **[No]**
- 455 4. If you are using existing assets (e.g., code, data, models) or curating/releasing new assets...
 - 456 (a) If your work uses existing assets, did you cite the creators? **[Yes]**
 - 457 (b) Did you mention the license of the assets? **[Yes]** See our GitHub:
458 github.com/chengtan9907/OpenSTL
 - 459 (c) Did you include any new assets either in the supplemental material or as a URL? **[Yes]**
460 See Appendix A.
 - 461 (d) Did you discuss whether and how consent was obtained from people whose data you’re
462 using/curating? **[Yes]**
 - 463 (e) Did you discuss whether the data you are using/curating contains personally identifiable
464 information or offensive content? **[N/A]**
- 465 5. If you used crowdsourcing or conducted research with human subjects...
 - 466 (a) Did you include the full text of instructions given to participants and screenshots, if
467 applicable? **[N/A]**
 - 468 (b) Did you describe any potential participant risks, with links to Institutional Review
469 Board (IRB) approvals, if applicable? **[N/A]**
 - 470 (c) Did you include the estimated hourly wage paid to participants and the total amount
471 spent on participant compensation? **[N/A]**